Acta Biomaterialia 134 (2021) 477–489

Contents lists available at ScienceDirect

Acta Biomaterialia

journal homepage: www.elsevier.com/locate/actbio

Full length article

A coarse-grained mechanical model for folding and unfolding of tropoelastin with possible mutations

Giuseppe Florio[a,b,*], Nicola M. Pugno[c,d], Markus J. Buehler[e,f,g], Giuseppe Puglisi[a]

[a] Dipartimento di Ing. Civile, Ambientale, del Territorio, Edile e di Chimica, Politecnico di Bari, Via Re David 200, 70126 Bari, Italy
[b] INFN Sezione di Bari, I-70126 Bari, Italy
[c] Laboratory of Bio-inspired, Bionic, Nano, Meta Materials & Mechanics, Department of Civil, Environmental and Mechanical Engineering, University of Trento, Italy
[d] School of Engineering and Materials Science, Queen Mary University of London, UK
[e] Laboratory for Atomistic and Molecular Mechanics, Massachusetts Institute of Technology, 77 Massachusetts Avenue, Room 1-165, Cambridge, MA 02139, USA
[f] Center for Materials Science and Engineering, Massachusetts Institute of Technology, 77 Massachusetts Avenue, Cambridge, MA 02139, USA
[g] Center for Computational Engineering, Massachusetts Institute of Technology, 77 Massachusetts Avenue, Cambridge, MA 02139, USA

ARTICLE INFO

Article history:
Received 3 March 2021
Revised 13 July 2021
Accepted 15 July 2021
Available online 22 July 2021

Keywords:
Coarse-grained modeling
Tropoelastin
Protein folding
Mutations
Force-elongation diagram

ABSTRACT

We propose a simple general framework to predict folding, native states, energy barriers, protein unfolding, as well as mutation induced diseases and other protein structural analyses. The model should not be considered as an alternative to classical approaches (Molecular Dynamics or Monte Carlo) because it neglects low scale details and rather focuses on global features of proteins and structural information. We aim at the description of phenomena that are out of the range of classical molecular modeling approaches due to the large computational cost: multimolecular interactions, cyclic behavior under variable external interactions, and similar. To demonstrate the effectiveness of the approach in a real case, we focus on the folding and unfolding behavior of tropoelastin and its mutations. Specifically, we derive a discrete mechanical model whose structure is deduced based on a coarse graining approach that allows us to group the amino acids sequence in a smaller number of 'equivalent' masses. Nearest neighbor energy terms are then introduced to reproduce the interaction of such amino acid groups. Nearest and non-nearest neighbor energy terms, inter and intra functional blocks are phenomenologically added in the form of Morse potentials. As we show, the resulting system reproduces important properties of the folding-unfolding mechanical response, including the monotonic and cyclic force-elongation behavior, representing a physiologically important information for elastin. The comparison with the experimental behavior of mutated tropoelastin confirms the predictivity of the model.

Statement of significance

Classical approaches to the study of phenomena at the molecular scale such as Molecular Dynamics (MD) represent an incredible tool to unveil mechanical and conformational properties of macromolecules, in particular for biological and medical applications. On the other hand, due to the computational cost, the time and spatial scales are limited. Focusing of the real case of tropoelastin, we propose a new approach based on a careful coarse graining of the system, able to describe the overall properties of the macromolecule and amenable of extension to larger scale effects (protein bundles, protein-protein interactions, cyclic loading). The comparison with tropoelastin behavior, also for mutations, is very promising.

1. Introduction

The possibility of predicting the mechanical behavior of protein molecules is crucially important in different fields such as biomaterials design and the understanding of biological processes [1–3]. However, conventional simulation methods such as

* Corresponding author at: Dipartimento di Ing. Civile, Ambientale, del Territorio, Edile e di Chimica, Politecnico di Bari
E-mail addresses: giuseppe.florio@poliba.it (G. Florio), nicola.pugno@unitn.it (N.M. Pugno), mbuehler@MIT.EDU (M.J. Buehler), giuseppe.puglisi@poliba.it (G. Puglisi).

https://doi.org/10.1016/j.actbio.2021.07.032
1742-7061/

molecular dynamics (MD) can be computationally expensive and limit the accessible space and time scales, often below relevant scales. To address these shortcomings, here we formulate a new coarse-grained approach for the analysis of folding and unfolding phenomena and the possible influence of mutations, focusing on the special important case of tropoelastin. Aimed at a significant reduction of the computational cost, with the purpose of considering complex phenomena out of the range of application of classical approaches (MD or Monte Carlo), we choose to neglect details at the single amino acid scale and focus on the configurational and mechanical properties at the macromolecular scale.

After the coarse graining step, obtained by grouping several amino acids in fictitious particles, we introduce Morse type NN (nearest neighbor) and NNN (non-nearest neighbor) interactions, phenomenologically chosen to reproduce the folding/unfolding experimental behavior. While for this reason such an approach cannot be considered as an alternative to the classical MD and Monte Carlo approaches, it can be an important inspiration to such methods and experiments [4] together with a simplified low-scale model for multiscale analysis of protein materials in the spirit of [5]. As we show, the obtained model can reproduce important experimental effects and MD results [6–8] on tropoelastin folding and diseases. Considering that MD simulations, especially when multimolecular systems are considered, are often characterized by a huge computational effort, sometimes incompatible with the space and time size of effective molecular systems phenomena, we believe that our approach can provide a significant new perspective in this crucially important field.

2. Materials and methods

The model here proposed aims at a description of the fundamental process of folding and unfolding and mechanical behavior of protein macromolecules. To fix the ideas and show the effectiveness of the model we focus on the important case of tropoelastin unfolding and refolding phenomena and to the analysis of known mutation phenomena [7,9].

The followed approach is energetic. This means that the energy associated to conformational changes of the protein regulates the kinetics of the observed unfolded→folded conformational transition, with a 'multiscale' competition of the energy associated to primary, secondary and tertiary structures. In particular, the main energetic contributions which are considered to dominate the native state protein stability are the hydrophobic effect, hydrogen bonding, configurational entropy and electrostatic interactions. Here, the primary structure is described by strong Nearest Neighbor (NN) interactions, reproducing the covalent links in the amino acids chain. The secondary and tertiary structures are instead assigned by *weak* Non-Nearest Neighbor (NNN) interactions, reproducing non-covalent bonds between chain elements. The presence of the non-covalent bonds regulates the folded→unfolded transformation, the relative stability of the native configuration as well as the crucial protein to ligand interactions. Mutations induce variations of the binding site within the protein structure that can alter the protein functionality. A comment about the physical origin of our choice of the potential energies is in order. We distinguished the structure based on the hydrophobic or hydrophilic properties of the domains because their interaction is fundamental in tropoelastin folding as well as in the folding of several other proteins [10,11]: indeed the fast process of protein assembly during coacervation is typically dominated by hydrophobic effects. On the other hand, electrostatic interactions, neglected in our modeling, can be relevant in the case of slow coacervation phenomena (so called "off critical" regime) [12,13]. As a matter of fact, the model can be extended to include electrostatic effects in the considered long-range effective interaction.

The typical folded configuration is shown in Fig. 1(a) where the important building blocks that contribute to the functionality of the molecule are evidenced. In particular, we may identify the N-terminus, the coil, the hinge, the bridge, the foot and the C-terminus. The sequence of hydrophobic and hydrophilic domains [14] is shown in Fig. 1(b). We treat the protein in the surrounding solvent as classical particles interacting through empirical potential energy functions. Specifically (see *e.g.* [15]), we describe the macrosystem as a chain of interacting elements with strong "nearest neighbor" (NN) interactions and weak, longer range, interactions that we collectively denote as "Non-Nearest Neighbor" (NNN). Since the principal energetic component underlying the secondary and tertiary structure configurations is the (entropically driven) clustering of hydrophobic components, minimizing the interaction of nonpolar residues with the solvent, NNN interactions depend on the hydrophilic or hydrophobic characteristics of the interacting elements (see the potential energy function in Fig. 4(b)). In particular, we may observe that each hydrophobic and hydrophilic domain contains a variable number of amino acids. In order to qualitatively reproduce the folding and unfolding kinematics of this system, each particle represents a (sequential) group of amino acids. We fix an average number of amino acids per particle and then subdivide each protein domain in a corresponding number of particles [16] (see table 2 in the following). In principle, by increasing the number of particles we may attain more accurate results. On the other hand, it may be desirable to obtain good molecular scale results with a small number of particles in order to speed-up the numerical simulations and consider larger space and time scales.

Lastly, as we describe in detail in the following, we introduce NNN interactions between different blocks (for example, between the coil section and the bridge section) in order to phenomenologically recover the main properties of the tertiary structure folding kinematics. Roughly speaking, our aim is to deduce a model that, by calibrating the material parameters to reproduce the experimental behavior, is characterized by an energy manifold keeping the main features of the real one. Once the model is calibrated, several tests on possible mutations, mechanical response, intermolecular interactions, morphological transitions and so on can be analyzed. Possibly, the deduced prototypical behaviors of the molecule can be tested and improved through a synergic analysis with experimental techniques and 'guided' molecular dynamics simulations.

Specifically, we consider the dynamical response of a discrete system of $N = 99$ particles and compare its behavior with the tropoelastin behavior in [6–8]. We describe the interaction energy between particles through the classical choice of Morse potentials. The role of water is introduced by considering a viscous dissipative term also favoring the convergence of the numerical analysis to obtain stable equilibrium configurations starting from assigned out of equilibrium states.

More in detail, our numerical scheme corresponds to the solution of a system of $3N$ nonlinear ODE for a system with local and long-range interactions of the Morse type (see Fig. 2 (b))

$$V_{ij} = D_{ij}\left(1 - e^{-\alpha_{ij}\left(r_{ij} - r_{ij}^0\right)}\right)^2, \tag{1}$$

where r_{ij} is the distance between particles i and j, α_{ij} is a control parameter for the width of the potential, r_{ij}^0 is the equilibrium distance and, finally, D_{ij} represents the well depth. All parameters have been carefully tuned to reproduce the experimental behavior and previous molecular dynamics simulations in [6–8] and are reported in Table 1. Observe that in this paper we are only interested in the possibility of a qualitative description of the structural and mechanical properties of the system reproducing the experimental behavior of the tropoelastin, whereas a direct calibration of the parameter on the experiments would give a fully quanti-

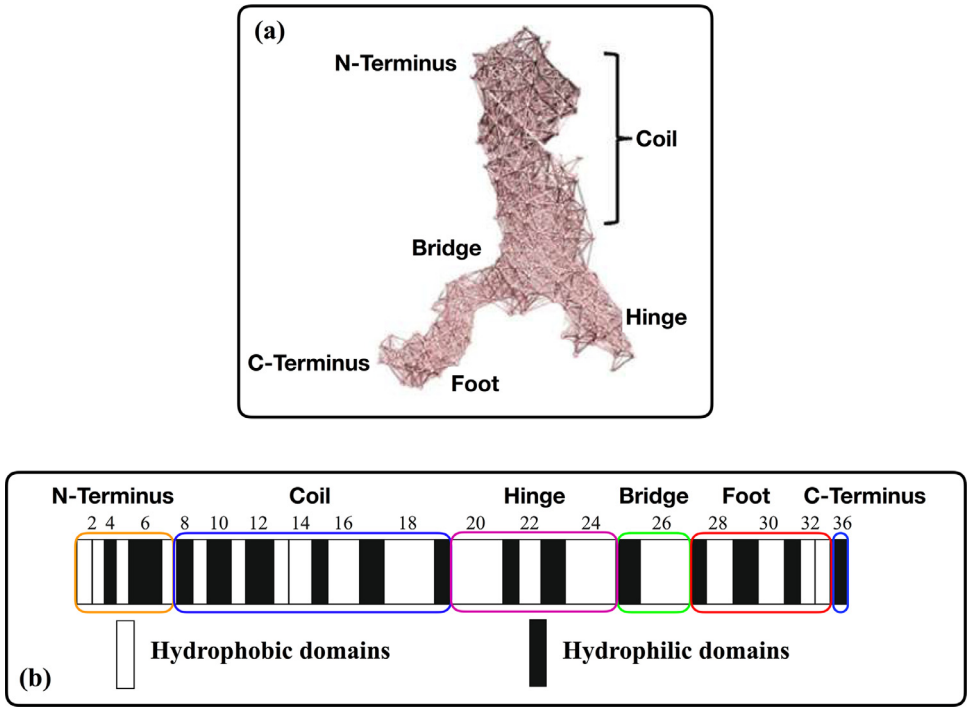

Fig. 1. (a) Typical folded configuration of tropoelastin with highlighted the main important blocks contributing to the functionality of the molecule: N-terminus, coil, hinge, bridge, foot and C-terminus (adapted from Ref. [29]).
(b) Sequence of hydrophobic and hydrophilic domains (see Ref. [14,21,29], adapted from [21]). Here and in the following figures we marked the functional blocks using different colors.

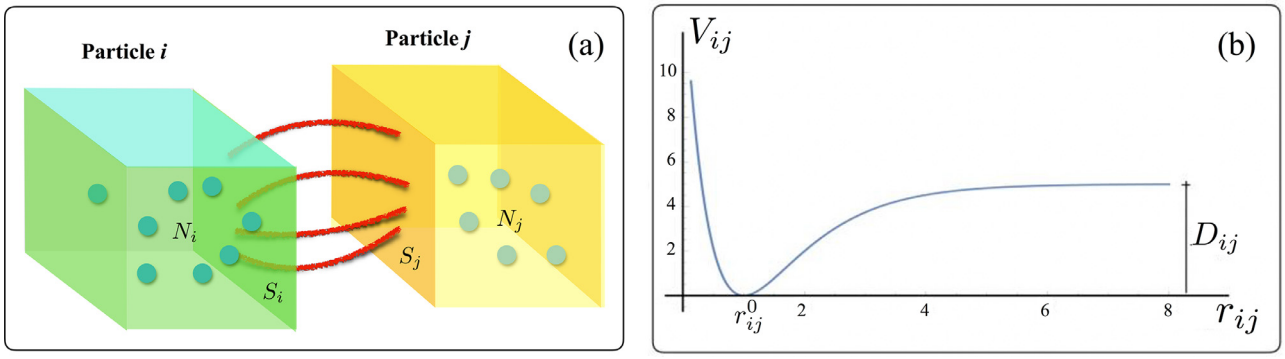

Fig. 2. (a) Schematic representation of the interaction between the particles of the model. Each cubic box represents a group of amino acids modelled as a single particle. The interaction energy between particles represents the average interaction among two different groups of amino acids. This energy is proportional to the product of the areas S_i and S_j facing each other. The volume V_j of a box is proportional to the number N_j of contained amino acids. The length size l_j scales as $l_j \propto N_j^{1/3}$. Thus, one has $S_j = l_j^2 \propto N_j^{2/3}$ and the interaction energy V_{ij} between particles i and j scales as $V_{ij} \propto S_i S_j \propto N_i^{2/3} N_j^{2/3}$.
(b) Morse potential between particles i and j has the form $V_{ij} = D_{ij}\,(1 - e^{-\alpha_{ij}(r_{ij} - r_{ij}^0)})^2$where r_{ij} is the distance between the particles i and j, α_{ij} *is* the parameter controlling the width of the potential, r_{ij}^0 is the equilibrium distance and D_{ij} is the well depth.

Table 1
Values of the parameters for the potential energies used in the simulations.

Potential	D_{ij}^0	α_{ij}	r_{ij}^0	r_{ij}^0 (mutation)
V_{NN}	1000	0.1	1	1
V_{NNN} (hydrophobic)	0.02	0.5	3	3
V_{NNN} (hydrophilic)	0.003	0.5	4	4
V_{block}	0.8	0.5	8	5
V_{block} $(coil - bridge)$	0.6	0.1	7	9

tative description. In this perspective, all material parameters are non-dimensional, being their ratio the only important factor. All these parameters depend on the nature of the interaction. In particular, we consider NNN interactions proportional to masses with $D_{ij} = N_i^{2/3} N_j^{2/3} D_{ij}^0$ where D_{ij}^0 depends, as already explained, on the (previously introduced) types of interaction, whereas N_i and N_j represent the number of amino acids considered in the particle i and j, respectively. The choice of the exponent derives from the following scaling argument. Let us consider each particle as a cubic box containing an assigned number of amino acids, see Fig. 2. The value of each N_i and the corresponding domain are detailed in Table 2. We suppose that the interaction energy between two boxes is proportional to the product of the areas S_i and S_j facing each other. If the volume V_j of a box is proportional to the number N_j of amino acids, then the length size l_j scales as $l_j \propto N_j^{1/3}$. Therefore, we have $S_j = l_j^2 \propto N_j^{2/3}$ so that the interaction energy V_{ij} between particles i and j scales as $V_{ij} \propto S_i S_j \propto N_i^{2/3} N_j^{2/3}$.

Table 2
Domain structure of tropoelastin, see also Fig. 1(b). For each domain we include the number of amino acids, the number of particles used in the simulation for the description of the domain, the mass of each particle in the group (the mass corresponds to the number of amino acids represented by the particle). Domain 22 is excluded because quiescent in mammalian tropoelastin [6].

Domain	Number of amino acids	Number of particles	Masses of particles
2	18	3	6-6-6
3	9	1	9
4	12	2	6-6
5	12	2	6-6
6	31	4	8-8-8-7
7	16	2	8-8
8	18	3	6-6-6
9	16	2	8-8
10	22	3	7-7-8
11	10	1	10
12	24	3	8-8-8
13	14	2	7-7
14	20	3	7-7-6
15	18	3	6-6-6
16	30	4	7-7-8-8
17	20	3	7-7-6
18	49	7	7-7-7-7-7-7-7
19	18	3	6-6-6
20	55	8	7-7-7-7-7-7-7-6
21	14	2	7-7
23	19	3	6-6-7
24	48	5	8-8-8-8-8-8
25	21	3	7-7-7
26	42	5	7-7-7-7-7-7
27	13	2	6-7
28	24	3	8-8-8
29	20	3	7-7-6
30	25	3	8-8-9
31	13	2	6-7
32	18	3	6-6-6
33	15	2	7-8
36	14	2	7-7

The system of $3N$ ODE governing the dynamics of the system is given by

$$m_i \ddot{\boldsymbol{r}}_i = -\gamma \dot{\boldsymbol{r}}_i + \sum_{j=1, j\neq i}^{N} \boldsymbol{F}_i^{(j)}, \quad i = 1, \ldots, N, \tag{2}$$

with $\boldsymbol{r}_i$ the position vector of the i-th particle. In the previous system the value of each mass m_i is equal to N_i and γ is a viscosity coefficient used to let the system reach an equilibrium configuration (the adopted values are reported in the figures). Force terms are obtained as

$$\boldsymbol{F}_i^{(j)} = -\nabla_i V_{ij}. \tag{3}$$

Local (NN) and non-local (NNN) interactions have the following structure (see the scheme in Fig. 3). First, we consider strong NN interactions involving consecutive particles at distance r (continuous red lines in Fig. 3 (a)); the resulting force acts also between consecutive particles that belong to different domains and blocks (N-terminus, coil, hinge, bridge, foot, C-terminus). We then consider NNN interactions among particles contained in a block (dashed lines in Fig. 3 (a); in order not to burden the picture, we have drawn only some NNN interactions as an example). In this case, we considered the possibility that the interaction takes place between two particles in three different scenarios: 1) both particles in a hydrophobic domain, 2) both particles in a hydrophilic domain, 3) one particle in a hydrophilic domain and the other particle in a hydrophobic domain. In particular, NNN energy terms describe stronger interactions inside the hydrophobic domains so to favor cross linking effects and inducing the observed clustering effect. Weaker energy terms describe the interaction between hydrophilic particles and between domains with different nature (hydrophobic and hydrophilic).

Finally, the different blocks interact among them through an energy term that is responsible for the final shape of the system. In particular, this interaction takes place through a coupling between the first and last particle in block i and the first and last particle in block j (see Fig. 3 (b)), respectively. The interactions between blocks act as a force conjugated to a collective variable given by the block distance. Finally, we remark that the N-terminus and C-terminus do not experience NNN interactions with other blocks. This choice has been made to reproduce a final configuration qualitatively similar to the observed tropoelastin configuration and reduce the number of parameters in the model.

In Fig. 4 we plot the different interaction energies used in the simulation with the corresponding parameters reported in Table 1. In particular, Fig. 4(a) shows the NN potential energy V_{NN}. In Fig. 4(b) we draw the energy potential V_{NNN} that describes the interaction among NNN particles contained in a block. Observe in particular the different behavior for hydrophobic and hydrophilic domains that we described above. In Fig. 4(c) we represent the potential energy V_{block} between different blocks. A comment is in order. The interaction taking place between the coil block and the bridge block is different. This choice has been made in order to improve the similarity between the numerical and observed folded configuration of tropoelastin. Moreover, as detailed in the following section, we use this energy term to reproduce the effect of mutation of residue 515 in the bridge [8,17] and subsequent modifications in the final conformation of tropoelastin.

Our model is based on the underlying assumption (see *e.g.* [18]) that the native conformation represents the global energy minimum configuration. As pointed out in [19], different trajectories, with different (high energy) transition states and energy barrier, typically lead to the same (minimum energy) native configuration.

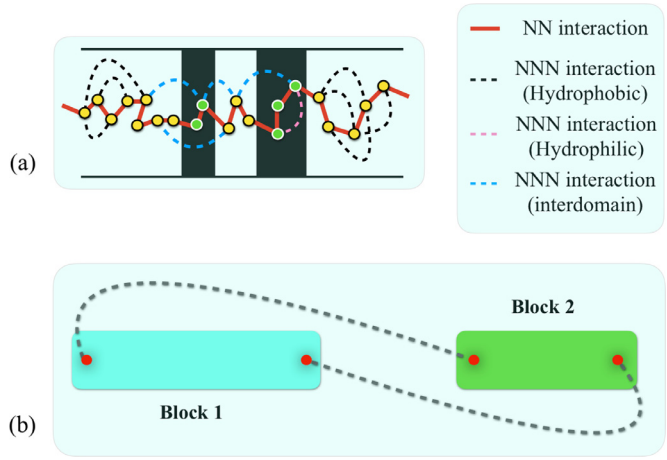

Fig. 3. (a) Scheme of the interactions among particles in a functional block. Strong NN interactions (continuous red) involve consecutive particles at distance r in a block and consecutive particles of different blocks (N-terminus, coil, hinge, bridge, foot, C-terminus). NNN interaction (dashed lines) involves particles contained in a block; for simplicity, we have drawn only some NNN interactions as an example. We consider three possible interactions of this kind: 1) both particles in a hydrophobic domain, 2) both particles in a hydrophilic domain, 3) one particle in a hydrophilic domain and the other particle in a hydrophobic domain. NNN energy terms describe stronger interactions inside the hydrophobic domains in order to favor cross linking and induce the observed clustering effect. A weaker energy term describes the interaction between particles in domains with different nature (hydrophobic and hydrophilic).
(b) Scheme of the interaction between functional blocks: this interaction takes place with a nonlocal energy term coupling the first and last particle in block i with the first and last particle in block j, respectively. N-terminus and C-terminus do not experience NNN interactions with other blocks. These choices, based on the existence of functional blocks and secondary/tertiary structures, have been calibrated to reproduce a final configuration qualitatively similar to the observed tropoelastin configuration and reduce the number of parameters in the model.

As a result, we may deduce that there is no unique pathway of folding and no unique intermediate, partially folded state. These states are close in structure to the native form and thereby lead to the typical assumption of the existence of a unique transition state. Once the barrier is overcome, folding occurs following the steepest descending path to the global energy minimum leading to the folded native state. Based on this qualitative description, we may argue that the efficacy of the proposed approach is that we are able to phenomenologically reproduce an energy manifold keeping the main energetic properties of the real energy manifold and in particular of the energy of the intermediate and native configurations.

Our dynamical strategy is described in Fig. 5 where we observe the typical evolution during the folding transition of the kinetic E_k and potential V energies as functions of time. First, we perturb the system in such a way that it is able to overcome the initial large energy barrier of the unfolded state. Loosely, the underlying hypothesis is the same assumed as a possible justification of the Levinthal paradox [20] based on the idea that protein folding is under a 'kinetic' control with the multiple folding pathways leading to the native states. In our model this assumption is verified *a fortiori* by observing a two-steps transition leading first to the secondary structure nucleation, followed by the tertiary structure nucleation. We have observed that both the kinetics and the energy levels of these two steps are largely and remarkably independent from the initial perturbed state. Roughly, once the system is perturbed, it is free to evolve and dissipate the excess energy to reach one of these isoenergetic states that then all transform to a unique folded state corresponding to the native configuration.

3. Results

We now test the efficacy of the proposed model in describing known experimental effects regarding folding, unfolding and mutation in tropoelastin reported in the literature [7,8,21,22].

3.1. Folding dynamics

We performed numerical simulations for a dynamical system of $N = 99$ particles, each describing a group of amino acids, interacting through the local and nonlocal energies previously introduced (see also Table 1 and 2 for details about the correspondence among particles and the groups of amino acids). In Fig. 5 we show the diagrams of the kinetic and potential energies during the system dynamical evolution. We mark the regions, denoted by S_1, S_2, S_3 and S_4, where the kinetic energy increases (and the potential energy decreases). Each step corresponds to a conformational transition of tropoelastin secondary and tertiary structure as shown in Figs 5. Schematically, the proposed dynamical system describes the following unfolded→folded transition strategy. First the chain dissipates the energy of the initial perturbation (sufficient to overcome the energy barrier allowing the folding process). This leads to a sudden decrease of the potential energy with the system still without 'clear' secondary structure. After this transition regime, due to the dissipative energy term, the system starts to follow the (steepest descending) path to the native conformation. Subsequently, the secondary structure is formed in sequential steps (S_1, S_2, S_3). Finally, the molecule relaxes in the native state minimum energy configuration (S_4) passing, as described in Fig. 6, through a 'torsional' rotation of the final block, reproducing the observed tropoelastin tertiary structure. Thus, according with our numerical result, the folding dynamics reflects the so called 'framework model' of protein folding [23]. Indeed, the system does not evolve continuously from the unfolded to the folded, native state, whereas it is characterized by successive abrupt conformational transitions (see

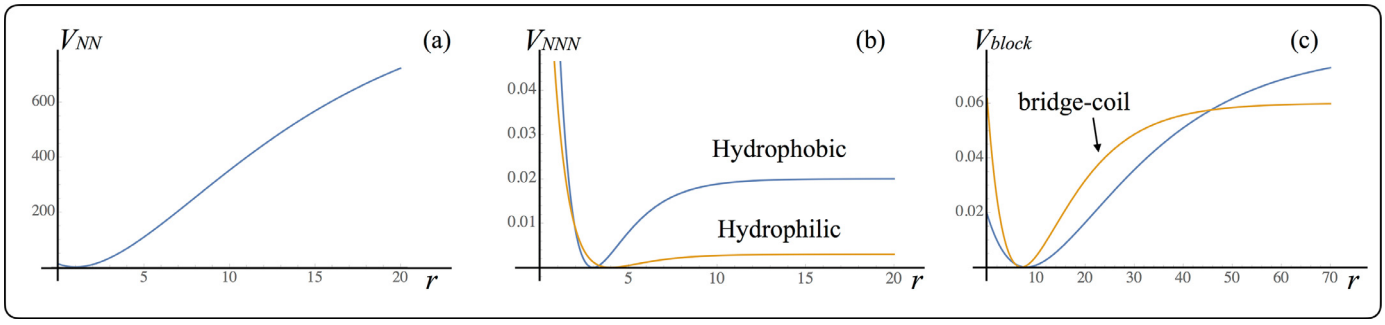

Fig. 4. Potentials energies considered for the different interactions. (a): NN potential energy V_{NN}. (b): nonlocal energy potential V_{NNN} describing the interaction among NNN particles contained in a block; the potentials for hydrophobic and hydrophilic interaction is different (c): nonlocal interactions energy potential V_{block} between blocks. The interaction taking place between the coil block and the bridge block is different.

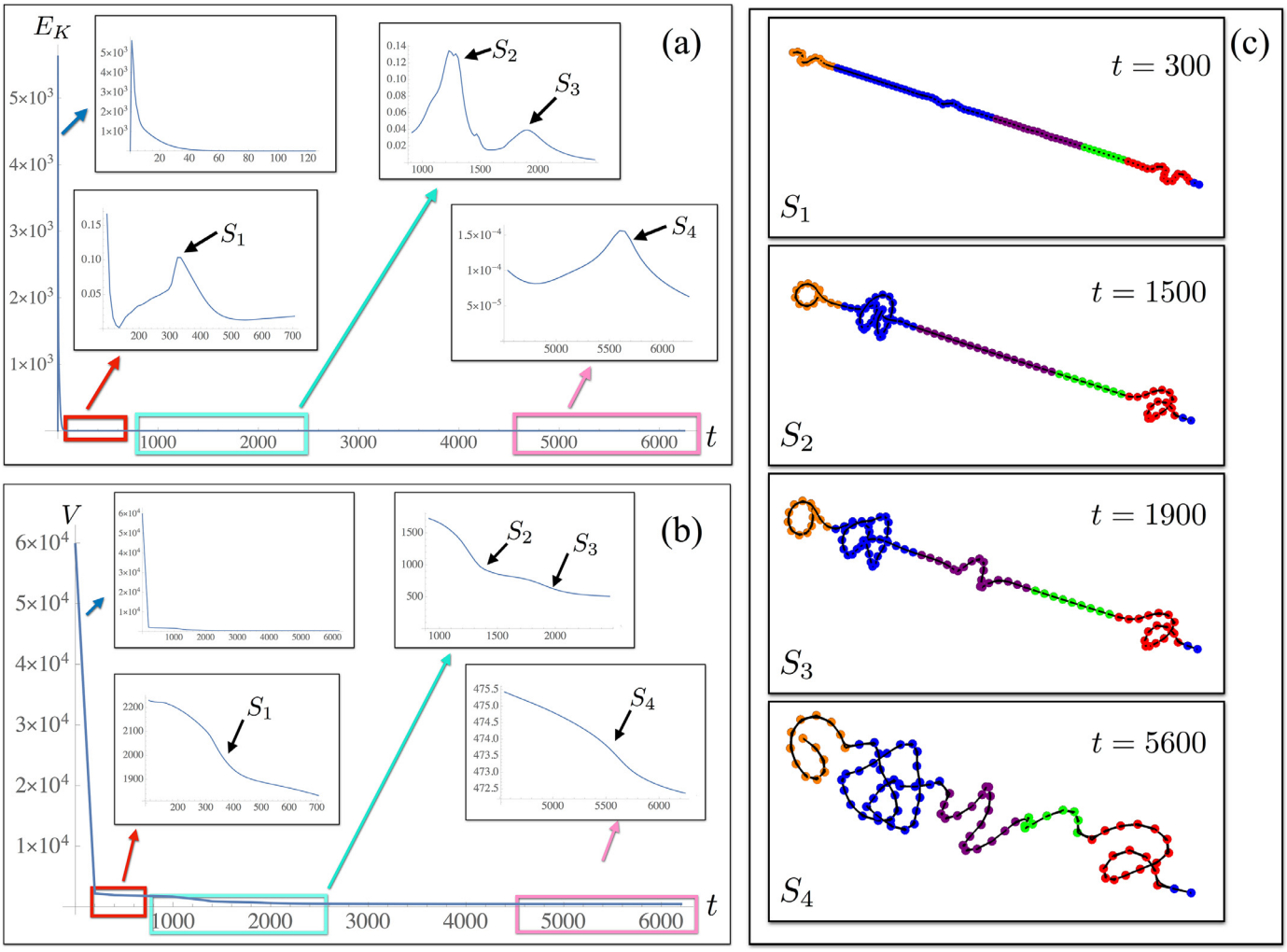

Fig. 5. Kinetc (a) and potential energy (b) evolution during the folding of tropoelastin to the native state: discontinuous transitions are evidenced by magnifications. We have marked the regions, denoted by S_1, S_2, S_3 and S_4, where the kinetic energy increases (and the potential energy decreases). Each step corresponds to a conformational transition reported in (c). First the chain dissipates the energy of the initial perturbation (assumed sufficient to overcome the energy barrier leading to the transition state). This corresponds to a sudden decrease of the potential energy with the system still without clear secondary structure nuclei. After this transition regime, due to the dissipative energy term in the equations of motion, the system follows the path to the native conformation (Fig. 6). See also the animation in the Supplementary Materials. Here and in the other figures, the parameters used for the simulations are those reported in Table 1 and 2 with the dissipation parameter γ=5. Different functional blocks are identified by different colors (see the caption in Fig. 1).

also the video in the Supplementary Materials). In particular we may observe the high energy difference between the initial unfolded state and the folded configuration with defined secondary structure. On the other hand, the successive transition involving tertiary structure rearrangement is characterized by a much lower energy difference.

In Fig. 7 we compare the initial and final configurations obtained after the folding. Interestingly, by varying both the initial perturbation at fixed non equilibrium end-to-end chain length and even by considering significantly different non equilibrium end-to-end length, our model shows that the system is always characterized by the same energetic and folding behavior (almost identical energy jumps and secondary structure states sequence) leading to the formation of the same primitive structure. For example, in Fig. 8 we show the energy evolution of the system starting from two different initial configurations with approximately 50% larger end-to-end initial length in the second case as compared with the first one. Observe that the dynamical behavior is highly reproducible with similar energies corresponding to the intermediate configurations in both cases reproducing the ones shown in Fig. 5(c). In particular, according with the previously described scheme, independently from the initial conditions or from the initial end-to-end length, the system 'falls down' after the initial energy jump to different configurations characterized by almost the same energy. The kinetic energy is then dissipated to attain the final nucleation of the secondary structure and finally for the final formation of the tertiary structure. The final conformation of the native configuration is independent from the initial conditions. Interestingly, also the time scales are independent from the initial condition. Finally, we considered a different coarse-graining scheme. Specifically, we included a different discretization, doubling the number of particles with half of the mass with respect to the previously shown discretization. We remark that we have not modified the values of the parameters of the Morse potentials, but only the values of the minimum distances of the NN interactions that have been coherently halved. The results are shown in Fig. 9 where we compare the previous discretization (left figure) and the new one (right figure). We observe that the system is stable under this rescaling and the final folded configurations show the same qualitative behavior and very similar quantitative features both from the topological and energetical point of view. Of course, such a refinement would require a new calibration of the

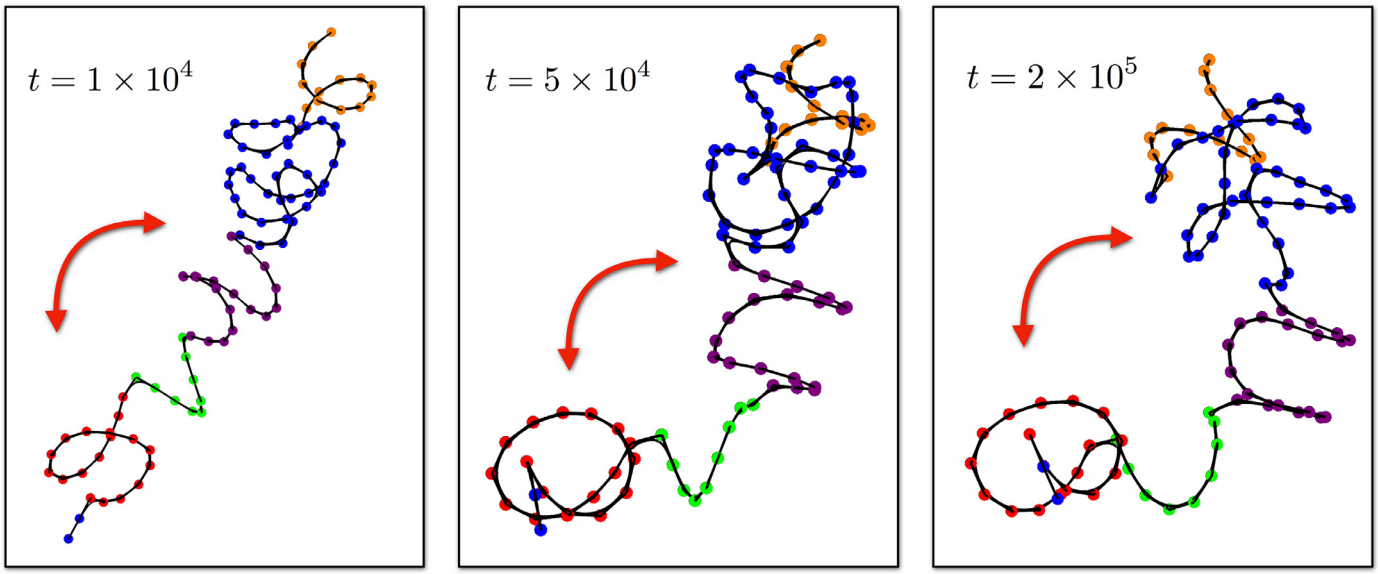

Fig. 6. Evidence of the tertiary structure formation in the final part of the folding transition: rotation of the blocks induced by the potential V_{block}. Different functional blocks are identified by different colors (see the caption in Fig. 1).

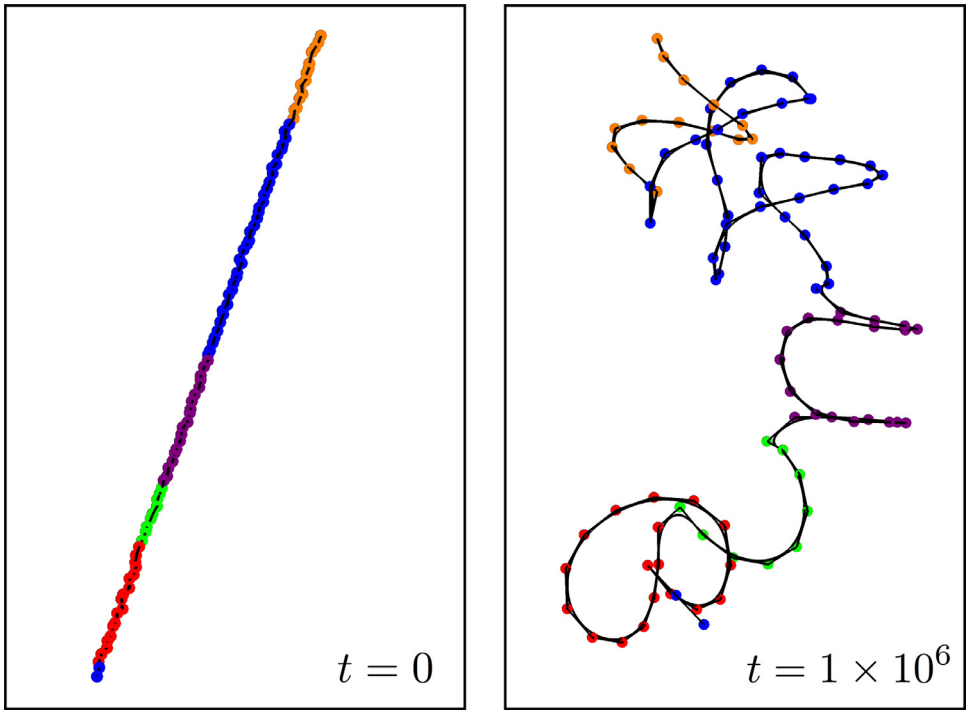

Fig. 7. Example of unfolded→folded transition with the initial and final configurations obtained after the folding. Different functional blocks are identified by different colors (see the caption in Fig. 1).

parameters for a better quantitative accordance, but the aim of this analysis is only to show the "stability" of the results with respect to the coarse graining scheme. This result is important because the refinement of coarsening of the proposed model will depend on the specific considered system with different types and number of molecular interactions.

The described results reflect the observation [24] that the global stability of the folded configuration is mainly regulated by the energy of the folded regions of the most probable partially folded conformations and that cooperative effects are maximal at the midpoint of the folding-unfolding transition [24]. Moreover, in accordance with the results reported in [25], the system shows two different relaxation phases with a 'fast' transition corresponding to the secondary structure formation and a 'slow' transition corresponding to the tertiary structure formation. As observed in [25] there are three orders of magnitude of difference in the transformation rates. The overall behavior can be also deduced by the movie reported in the SM. Observe also that the initial energy gives a measure of the energy barrier that the system has to overcome to nucleate the transition state and thus it may also give a measure of the rate constant of the transition based on Arrhenius type formulation [26]. We also remark that the described sequential morphological transition is observed in our numerical experiments also in the reverse unfolding path (first the tertiary struc-

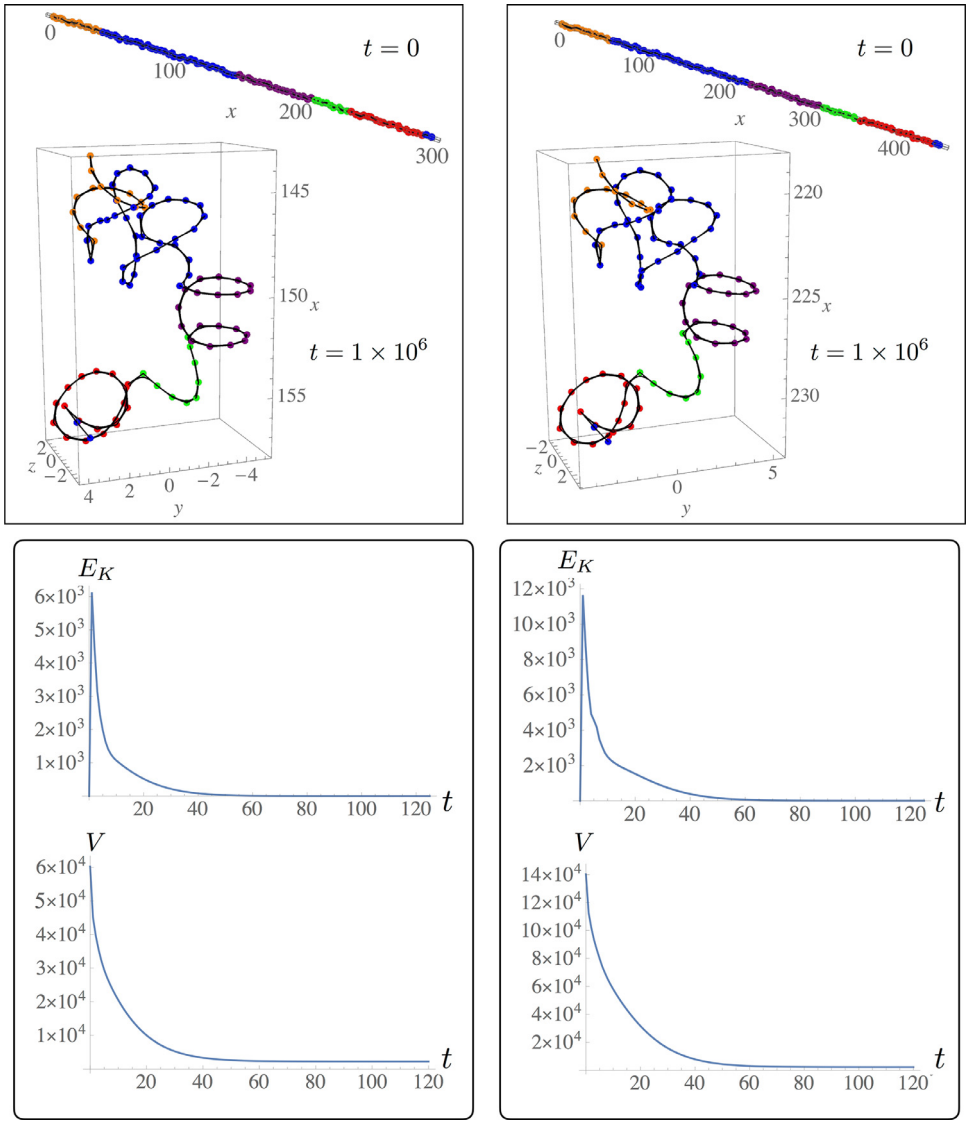

Fig. 8. Independence of the final folded configuration from the initial condition. The figures on the right corresponds to the initial end-to-end distance approximately 50% larger than the initial configuration on the left. From top to bottom initial unfolded configuration, final folded configuration, kinetic energy and potential energy. Different functional blocks are identified by different colors (see the caption in Fig. 1).

ture unfolds while the secondary structure is involved only later) in accordance with the results in [18]. Moreover, our results are in agreement with the observation [27] that the N-terminal domain is nucleated first and then it is stabilized by the interaction with the C-terminus. This stabilization effect is induced in our model by the NNN interactions inducing the protein torsion following the N and C nucleation and leading to the final configuration of the native state.

3.2. Force-elongation relation

In this section we focus on the important mechanical behavior in order to assess the possibility of analyzing also the force-induced unfolding of the native states. Specifically, we applied a constant force F to the first and last element along the chain axis (end-to-end vector) starting from a folded configuration obtained by previously described dynamical process. The resulting protein response is reported in Fig. 10, where we show the relation of the applied force with the projection of the end-to-end distance along the force direction d_x between these two elements of the chain. In this case we deduce the equilibrium configurations by applying an increasing force to the completely folded conformation and evaluating the corresponding elongation after molecule relaxation. As expected, increasing the applied force the system undergoes a reverse structural transition. The force elongation diagram shows sudden changes of the elongation d_x at almost fixed (transition) forces F corresponding to the breaking of secondary structures. The arrow in the figure corresponds to the persistence of the secondary structure in the coil block whose failing induces the subsequent sudden final increase of d_x. Notice that, after the complete unfolding of the tertiary and secondary structure, the curve displays an (experimentally observed) sharp increase due to the strong NN interactions.

In order to further test the model, we followed a different approach to obtain the force/end-to-end length curve. We applied a stepwise increasing force to a completely folded configuration. In this case we consider a monotonic loading with a fixed value of incremental force ΔF. Once again, after each increment of the force we let the system relax and we measure the corresponding end-to-end distance. Starting from the attained state, we apply again an increment ΔF at the new attained configuration. The procedure is repeated until full unfolding is reached.

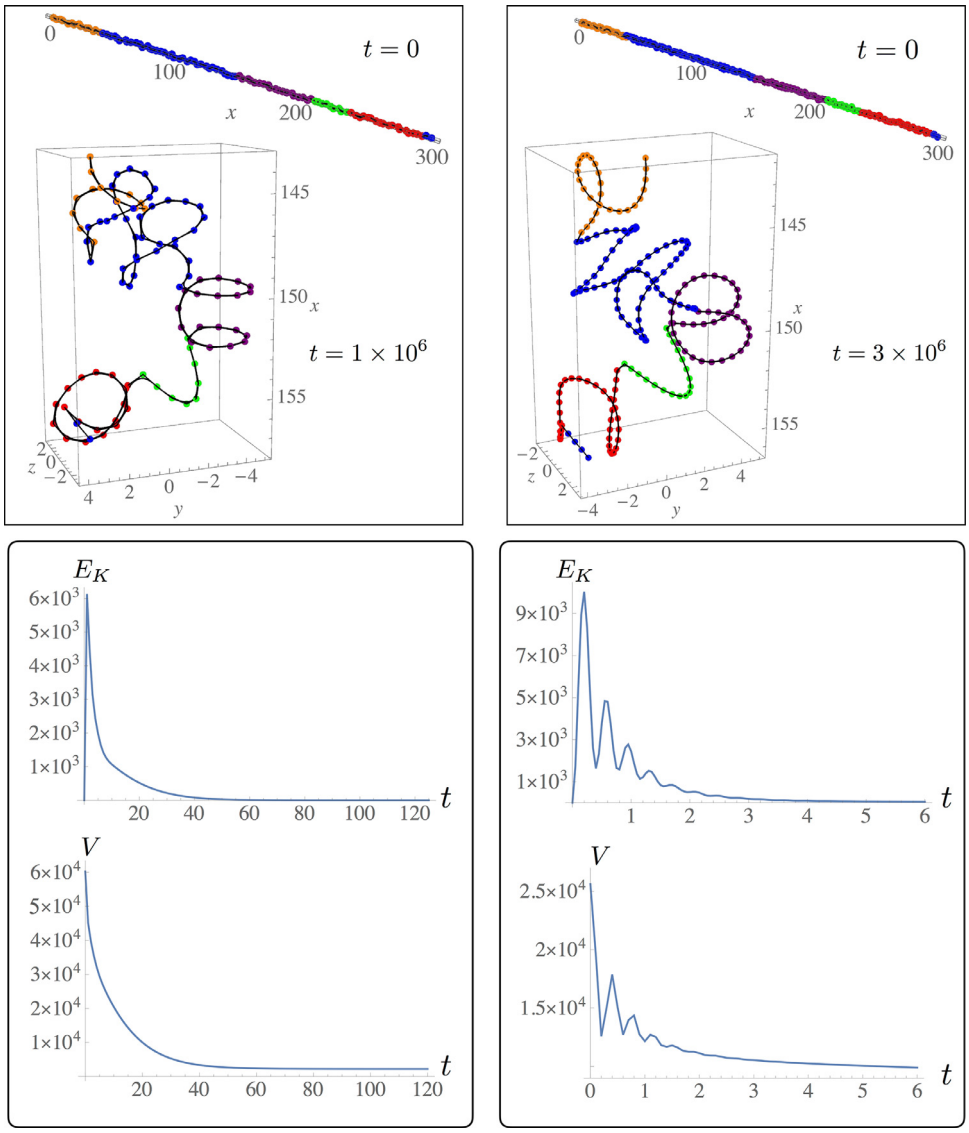

Fig. 9. Comparison of different coarse-graining schemes. Figures on the right correspond to doubling the number of particles with half of the mass with respect to discretization used for the results shown in the left figures. We have *not* modified the values of the parameters of the Morse potentials, but only the values of the minimum distances of the NN interactions have been halved. Different functional blocks are identified by different colors (see the caption in Fig. 1).

Then, we consider the molecule behavior under cyclic loading histories to analyze the reversibility or the hysteretical response (see the loading history in Fig. 11(a)). We may observe two different regimes shown respectively in Fig. 11(b) and Fig. 11(c). In the former we show loading/unloading force/elongation curves with a stepwise constant force in a low force regime Fig. 11(b). As can be expected, for low force cycles the behavior is practically elastic with no hysteresis. On the other hand, when we reach the full unfolding, the system shows a significantly different loading-unloading path that is associated to hysteresis and energy dissipation. In particular, in the case of higher forces in Fig. 11(c) the secondary structure is unfolded differently from the case in Fig. 11(b). Observe that in the figures are shown the paths corresponding to different values of the dissipation parameter γ. The curves are independent from this parameter except the final point of the unloading curve that, as the dissipation is increased, stops in a slightly longer final configuration. In particular, by decreasing γ we end up with a final configuration more and more similar to the initial one at the beginning of the loading path (with a final folded configuration largely similar to the initial one). The process in the low force regime corresponds to the unfolding of the tertiary structure as shown in the inset of the figure with the secondary structures unaffected. On the other hand, if we increase the value of the applied force, we observe a hysteresis phenomenon after the cycle is completed. Interestingly, according with our numerical analysis also hysteresis is not affected by the value of the dissipation parameter γ. This irreversible process corresponds to the sequential breaking of the secondary structures as shown in the inset whereas the folding-unfolding process in the tertiary structure is elastic. The general behavior of the force-elongation diagrams is consistent with the experimental and numerical results (see *e.g.* [28,29]). On the other hand, the presence of hysteresis is consistent with experimental results obtained in tropoelastin and elastin experiment in literature [30–34].

3.3. Effects of mutation

As another important test of the efficacy of the obtained model in describing and predicting important observed phenomena, we here show how it is possible to describe, once the parameters have

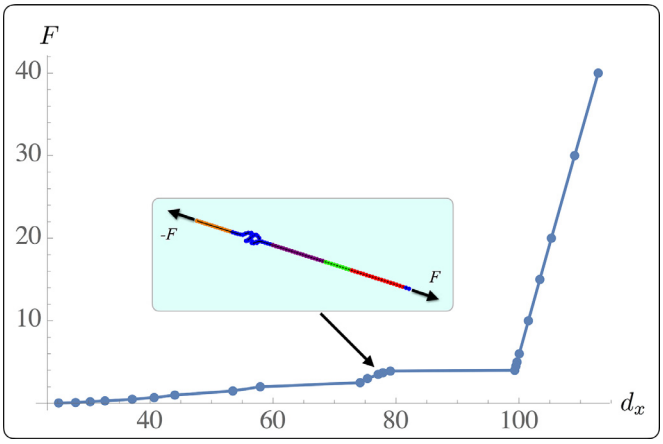

Fig. 10. Applied force as a function of the end-to-end distance d_x measured as its projection along the force direction. Each point in the plot is obtained as in the following description: we start from a completely folded conformation and apply a force F to both ends of the chain in opposite directions. After the system reaches the equilibrium configuration the value of d_x is measured. Then, a larger force is applied again starting from the folded state and the new equilibrium displacement is measured. After the complete unfolding of the tertiary and secondary structure, the curve displays a sharp increase due to the strong NN interactions. We also observe that the obtained sudden changes of d_x for small increases of F correspond to the breaking of the secondary structures. The interval marked by the arrow corresponds to the persistence of the secondary structure in the coil block that disappears in the subsequent force plateau. Different functional blocks are identified by different colors (see the caption in Fig. 1).

been calibrated as shown in previous section, the effects of possible mutations. In s particular we consider (see Fig. 12) the R515A mutation inside the block connecting the feet by modifying the long-range interaction as studied in [8]. We phenomenologically reproduced such mutation by increasing the value of the distance r_{ij}^0 of the long-range interaction between the bridge block and the coil block and decreasing the value of r_{ij}^0 among the other blocks. The obtained system shows a behavior reproducing the results reported in [6,8]. In particular we obtain a decrease of the average distance between the hinge and foot blocks (foot span). The averages are 4.90 and 3.83 (non-dimensional units) for the normal and mutated chain, respectively. Analogously, the average elongation of the foot block (measured as the distance between the beginning of foot block and the end of the C-terminus block) is 5.59 and 5.04 (non-dimensional units determined by the assigned Morse potentials) for the normal and mutated chain, respectively. This qualitative confirmation of the experimental behavior supports once again the possibility of describing crucial effects of the mutations on the conformation of the proteins with the consequent variation of coacervation. This result can find an explanation in the behavior of α-helices and β-sheets observed in MD [8]. In particular, the percentage of α-helices is increased and a more-ordered secondary structure is observed.

Finally, in Fig. 13 we show the response to a force applied to the end particles of the mutated system with respect to the behavior observed in Fig. 10 for the original system. Observe that the mutated system shows a tendency to maintain a more compact structure with smaller values of the end-to-end distance. This behavior is due to the larger value assigned to the equilibrium distance between coil and bridge inducing the hinge and the foot blocks to stay closer.

A comment is now in order. We have considered the effects of the particular mutation detailed above by modifying the long-range interaction between the coil and the bridge blocks. Of course, each other possible mutation would require the identification of relevant structural changes in the conformation of the protein so to associate this change to the parameters in the effective potential energies included in the model.

4. Discussion

We introduced a course-grained mechanical model able to describe the structural behavior of tropoelastin at the molecular scale. While the model neglects the details of single amino acids, we show the ability of analyzing global molecular properties, both mechanical and topological. In particular, the important folding-unfolding conformational transition, the force-elongation relation using different loading strategies both for loading and unloading, and the effect of mutations are successfully obtained.

To focus the attention on a real case, we considered the behavior of an important protein precursor of elastin: the tropoelastin. The model is able to reproduce the main experimental features observed in such protein. Several properties, in our opinion, are worth to mention. Our model, as compared to classical approaches based on MD, is numerically enormously advantageous thus offering the possibility of performing numerical experiments on large systems such as interacting molecules or protein bundles that are out of the range of applications of MD experiments. Our numerical tests showed the high morphological stability of the folded configuration starting from very different initial configurations. In particular, we tested initial configurations where the distance among the particles in the direction of one axis and the range of fluctuations along the other axes are 50% larger than in other numerical simulations, thus showing a robustness of the equilibrium folded configuration in agreement with the well-known stability of folded configurations of proteins (*e.g.*, tropoelastin). Moreover, we have changed the number of particles used in the simulations and rescaled the masses and coherently the distances where the nearest-neighbor potential energies are minima. We found that the final folded configuration is consistent with the previous results. This result indicates that the approach is mainly independent on the coarse-graining scheme and that it captures the main structural and energetic features of the system.

The folding process shows the formation in sequence of secondary and tertiary structure [35,36] in agreement with a “framework folding model”. In particular, our model qualitatively reproduces the ‘topological regions’ known in the folded configuration of tropoelastin [29]. In order to further investigate the effectiveness of the model, we considered the effect of mutation through a modification of the foot-coil block interaction. We observe a larger force in the mutated scheme needed to obtain a desired value of elongation. In other words, the mutation induces an increased rigidity of the system. This reflects the observation that in the case of a biological macromolecule such as tropoelastin, mutations of this form could affect its functionality and, in the end, hierarchical assembly [7].

We obtained a force-elongation diagram that shows an initial slight hardening, corresponding to the unfolding of the folded structure. After this stage one observes a sudden stiffness increase that is induced by the large stiffness of the NN interactions, dominant after the unfolding of tertiary and secondary structures (this reflects the experimental and numerical results in *e.g.* [28,29]). In the unfolding process at fixed force, we distinguish a low force regime where the behavior is mainly reversible and elastic elongation corresponds to the reversible tertiary structure unfolding. In this regime the system behaves as an elastic spring. For larger values of the assigned force the behavior is irreversible with a large hysteresis and dissipation that in the range of our numerical experiment is independent from both rate of loading and viscosity. This behavior is coherent with the experimental elastin behavior in [32] where the author observes that for temperature such that

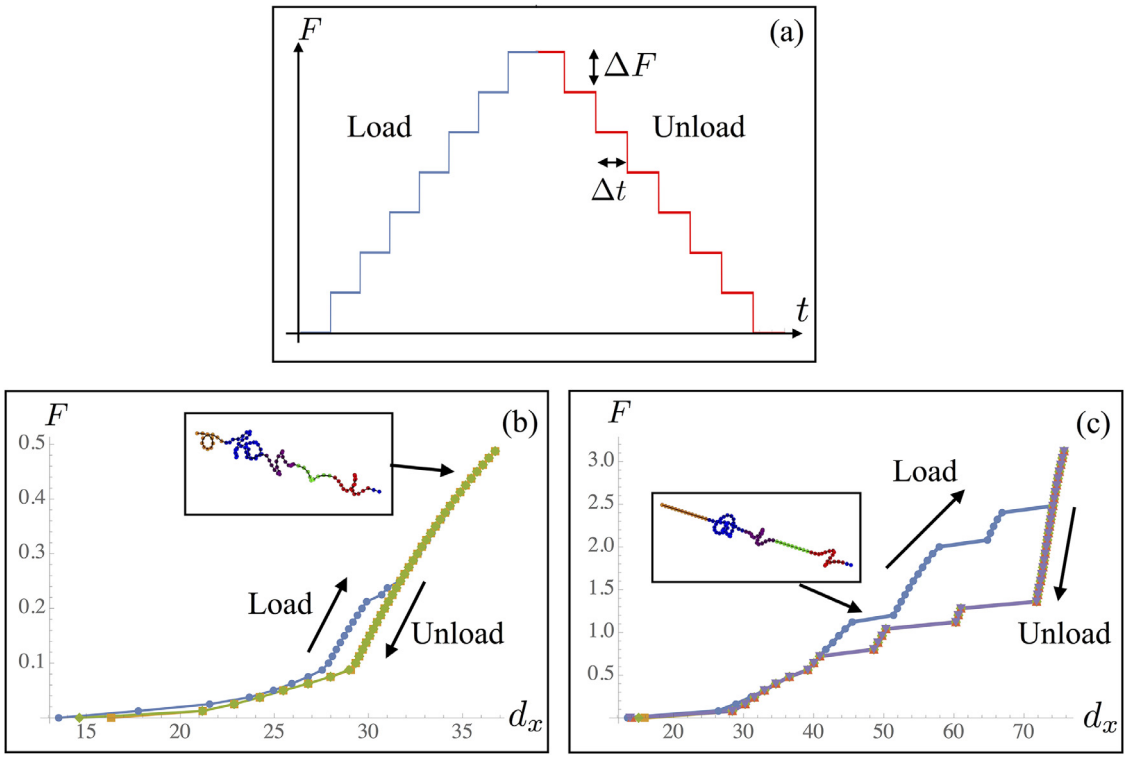

Fig. 11. Cyclic loading behavior of the tropoelastin molecule.
(a): Stepwise constant force applied to the ends of the chain to test the behavior of the system during a loading-unloading cycle. After the application of the force, the system can evolve for a time interval Δt until it reaches an equilibrium configuration. After this interval the force is increased (decreased during the unload process) by ΔF starting from the new attained conformation.
(b): Low maximum force cyclic behavior. During the unloading phase we considered different values of the dissipation parameter γ ($\gamma = 1$ and $\gamma = 5$); the reduction of this parameter corresponds to a final configuration more and more similar to the initial one at the beginning of the loading phase. The unfolding process in this regime corresponds to the breaking of the tertiary structure as shown in the inset with the secondary structures unaffected. Observe the (almost perfectly) elastic behavior of the system with almost no hysteresis and coincidence of loading and unloading paths. Different functional blocks are identified by different colors (see the caption in Fig. 1).
(c): High maximum force (hysteretic, dissipative) cyclic behavior. In this regime the phenomenon of hysteresis appears after the cycle is completed. Hysteresis is not affected by the value of the dissipation parameter γ (ranging from 5 to 0.5). This irreversible process corresponds to the sequential breaking of the secondary structures as shown in the inset. Different functional blocks are identified by different colors (see the caption in Fig. 1).

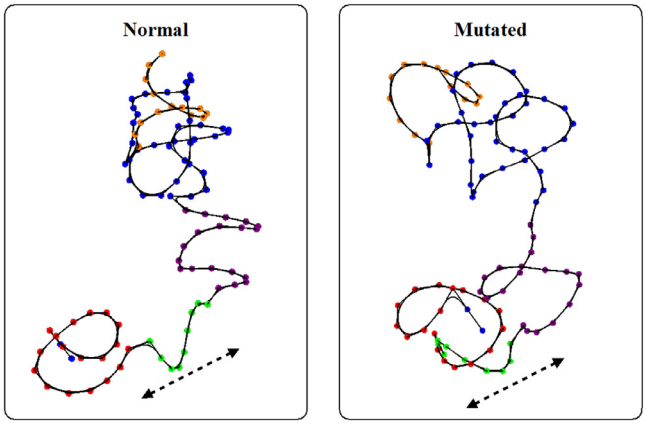

Fig. 12. Foot span: Example of final configurations in case of normal chain (left fig.) and mutated chain (right fig.). Mutation is introduced by modifying the long-range interaction, increasing the value of the distance r_{ij}^0 of the long-range interaction between the bridge block and the coil block and decreasing the value of r_{ij}^0 among the other blocks. The average distance between the hinge and foot blocks (foot span) changes from 4.90 to 3.83 (in non-dimensional units) for the normal and mutated chain, respectively. Analogously, the average elongation of the foot block is 5.59 and 5.04 for the normal and mutated chain, respectively. Different functional blocks are identified by different colors (see the caption in Fig. 1).

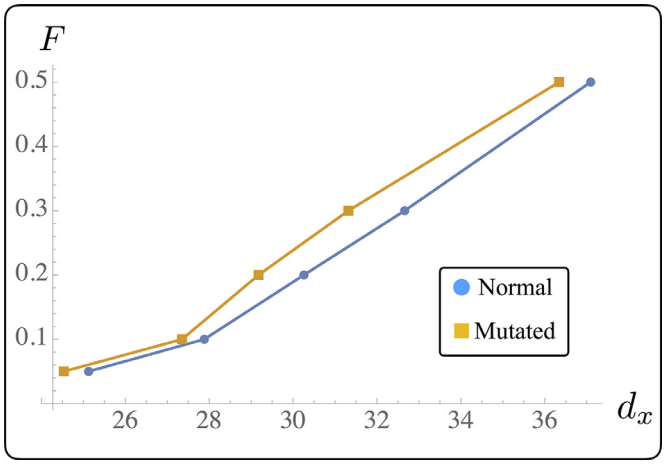

Fig. 13. Applied force vs end-to-end distance in the case of normal and mutated chain. The procedure for obtaining the plot is analogous to the one described in the caption of Fig. 10. The mutation is included as described in the text and in the caption of Fig. 12.

the hydrophobic effect is not activated and no secondary structure is present, the behavior is reversible. On the other hand, when the temperature induces the hydrophobic effect and secondary structure formation, large hysteresis is observed associated to the folding-unfolding transition of the secondary structure. We stress an important point of our approach. The calibration of the parameters has been based on the only reproduction of the final conformational structure of the folded system (wild-type and mutated).

Once fixed these parameters, we tested the model in order to obtain the force-elongation curves and the cyclic loading/unloading curves reproducing known experimental behavior. Thus, these results are not introduced *ab initio* and are emergent features of the model.

A comment about future research activity and the extension of the presented approach is in order. We see our approach as a starting point for the modeling of more complex systems that are out of the range of application of other classical methods such as Molecular Dynamics simulations due to computational effort. Thus, future work will be related to the validation of this model using parameters that can allow a quantitative comparison with numerical and experimental results. Moreover, it would be interesting to consider and analyze a system made of a chain of tropoelastin elements in order to test the behavior of a model of elastin.

Finally, one would like to extend this model to other macromolecules of interest for applications in biology and bio-inspired materials. The application to different systems will require the calibration of the local and long-range interaction potentials. On the other hand, some general features of the model (such as the scaling law characterizing the interaction strength between particles of the form $N^{2/3}$ or the role of hydrophobic effect in the folding process of several proteins) are general, suggesting that this approach can be adapted to other cases in order to consider different effects. We are thus confident that the proposed approach will deliver an important innovative tool to study significantly more complex structures, beyond the range of applications of present MD approaches.

Funding

MJB acknowledges support from the MIT-IBM AI lab, ONR (N000141612333 and N000141912375), AFOSR (FATE MURI FA9550-15-1-0514), as well as NIH (EB014976), as well as ARO (W911NF1920098). GF and GP have been supported by the Italian Ministry MIUR-PRIN project “Mathematics of active materials: From mechanobiology to smart devices” (2017KL4EF3). GF and GP are supported by GNFM (INdAM). GP and GF are also supported by the Italian Ministry MISE through the project RAEE SUD-PVP. GF is also supported by INFN through the project “QUANTUM”, by the FFABR research grant (MIUR) and the PON S.I.ADD. NMP is supported by the European Commission under the FET Open “Boheme” grant no. 863179, as well as by the Italian Ministry of Education, University and Research (MIUR) under the PON ARS01-01384- PROSCAN Grant and the PRIN-20177TTP3S.

Declaration of Competing Interest

The authors declare that they have no known competing financial interests or personal relationships that could have appeared to influence the work reported in this paper.

Supplementary materials

Supplementary material associated with this article can be found, in the online version, at doi:10.1016/j.actbio.2021.07.032.

References

[1] M.J. Cranford, S.W. Buehler, Biomateriomics ed., Springer, 2012. https://www.springer.com/gp/book/9789400716100.
[2] Z. Qin, M.J. Buehler, Structure and dynamics of human vimentin intermediate filament dimer and tetramer in explicit and implicit solvent models, J. Mol. Model. 17 (2011) 37–48, doi:10.1007/s00894-010-0696-6.
[3] M.J. Buehler, Y.C. Yung, Deformation and failure of protein materials in physiologically extreme conditions and disease, Nat. Mater. 8 (2009) 175–188, doi:10.1038/nmat2387.
[4] P.L. Freddolino, C.B. Harrison, Y. Liu, K. Schulten, Challenges in protein-folding simulations, Nat. Phys. 6 (2010) 751–758, doi:10.1038/nphys1713.
[5] D. De Tommasi, G. Puglisi, G. Saccomandi, Multiscale mechanics of macromolecular materials with unfolding domains, J. Mech. Phys. Solids 78 (2015) 154–172, doi:10.1016/j.jmps.2015.02.002.
[6] A. Tarakanova, Molecular Structure, Hierarchical Assembly And Stimuli-Responsive Mechanics of Tropoelastin and Elastin Biomaterials PhD Thesis, Molecular Structure, Hierarchical Assembly And Stimuli-Responsive Mechanics of Tropoelastin and Elastin Biomaterials, 2017, M.I.T., 2017.
[7] G.C. Yeo, A. Tarakanova, C. Baldock, S.G. Wise, M.J. Buehler, A.S. Weiss, Biomolecules: Subtle balance of tropoelastin molecular shape and flexibility regulates dynamics and hierarchical assembly, Sci. Adv. 2 (2016) 1–15, doi:10.1126/sciadv.1501145.
[8] A. Tarakanova, G.C. Yeo, C. Baldock, A.S. Weiss, M.J. Buehler, Molecular model of human tropoelastin and implications of associated mutations, Proc. Natl. Acad. Sci. USA 115 (2018) 7338–7343, doi:10.1073/pnas.1801205115.
[9] A. Tarakanova, J. Ozsvar, A.S. Weiss, M.J. Buehler, Coarse-grained model of tropoelastin self-assembly into nascent fibrils, Mater. Today Bio. 3 (2019), doi:10.1016/j.mtbio.2019.100016.
[10] R.D. Hills, C.L. Brooks, Hydrophobic Cooperativity as a Mechanism for Amyloid Nucleation, J. Mol. Biol. 368 (2007) 894–901, doi:10.1016/j.jmb.2007.02.043.
[11] A.W. Fitzpatrick, T.P.J. Knowles, C.A. Waudby, M. Vendruscolo, C.M. Dobson, Inversion of the balance between hydrophobic and hydrogen bonding interactions in protein folding and aggregation, PLoS Comput. Biol. 7 (2011), doi:10.1371/journal.pcbi.1002169.
[12] G.C. Yeo, F.W. Keeley, A.S. Weiss, Coacervation of tropoelastin, Adv. Colloid Interface Sci. 167 (2011) 94–103, doi:10.1016/j.cis.2010.10.003.
[13] H.X. Zhou, X. Pang, Electrostatic Interactions in Protein Structure, Folding, Binding, and Condensation, Chem. Rev. 118 (2018) 1691–1741, doi:10.1021/acs.chemrev.7b00305.
[14] R.H. Garrett, C.M. Grisham, Biochemistry, Brooks/Cole, Cengage Learning, 2013.
[15] H.S. Chan, K.A. Dill, Protein structure and stability, Annu. Rev. Biophys. Chem. 20 (1991) 447–490.
[16] A.R. Panchenko, Z. Luthey-Schulten, P.G. Wolynes, Foldons, protein structural modules, and exons, Proc. Natl. Acad. Sci. USA 93 (1996) 2008–2013, doi:10.1073/pnas.93.5.2008.
[17] G.C. Yeo, C. Baldock, A. Tuukkanen, M. Roessle, L.B. Dyksterhuis, S.G. Wise, J. Matthews, S.M. Mithieux, A.S. Weiss, Tropoelastin bridge region positions the cell-interactive C terminus and contributes to elastic fiber assembly, Proc. Natl. Acad. Sci. USA 109 (2012) 2878–2883, doi:10.1073/pnas.1111615108.
[18] T. Lazaridis, M. Karplus, New view of protein folding reconciled with the old through multiple unfolding simulations, Science 278 (1997) 1928–1931, doi:10.1126/science.278.5345.1928.
[19] R.L. Baldwin, Matching speed and stability, Nature 369 (1994) 183–184, doi:10.1038/369183a0.
[20] K.A. Dill, H.S. Chan, From levinthal to pathways to funnels, Nat. Struct. Biol. 4 (1997) 10–19, doi:10.1038/nsb0197-10.
[21] S.G. Wise, G.C. Yeo, M.A. Hiob, J. Rnjak-Kovacina, D.L. Kaplan, M.K.C. Ng, A.S. Weiss, Tropoelastin: a versatile, bioactive assembly module, Acta Biomater. 10 (2014) 1532–1541, doi:10.1016/j.actbio.2013.08.003.
[22] L.B. Sandberg, N.T. Soskel, T.B. Wolt, Structure of the elastic fiber: an overview, J. Invest. Dermatol. 79 (1982) 128–132, doi:10.1038/jid.1982.24.
[23] O.B. Ptitsyn, Kinetic and equilibrium intermediates in protein folding, Protein Eng. Des. Sel. 7 (1994) 593–596, doi:10.1093/protein/7.5.593.
[24] V.J. Hilser, D. Dowdy, T.G. Oas, E. Freire, The structural distribution of cooperative interactions in proteins: analysis of the native state ensemble, Proc. Natl. Acad. Sci. USA 95 (1998) 9903–9908, doi:10.1073/pnas.95.17.9903.
[25] R. Gilmanshin, S. Williams, R.H. Callender, W.H. Woodruff, R.B. Dyer, Fast events in protein folding: relaxation dynamics of secondary and tertiary structure in native apomyoglobin, Proc. Natl. Acad. Sci. USA 94 (1997) 3709–3713, doi:10.1073/pnas.94.8.3709.
[26] D. Scalley, M.L. Baker, Protein folding kinetics exhibit an Arrhenius temperature dependence when corrected for the temperature dependence of protein stability, PNAS 94 (1997) 10636–10640. doi: 10.1073/pnas.94.20.10636.
[27] K.P. Murphy, Stabilization of protein structure, Methods Mol. Biol. 168 (2001) 1–16, doi:10.1385/1-59259-193-0:001.
[28] C. Baldock, A.F. Oberhauser, L. Ma, D. Lammie, V. Siegler, S.M. Mithieux, Y. Tu, J.Y.H. Chow, F. Suleman, M. Malfois, S. Rogers, L. Guo, T.C. Irving, T.J. Wess, A.S. Weiss, Shape of tropoelastin, the highly extensible protein that controls human tissue elasticity, Proc. Natl. Acad. Sci. USA 108 (2011) 4322–4327, doi:10.1073/pnas.1014280108.
[29] A. Tarakanova, S. Chang, M.J. Buehler, Computational materials science of bionanomaterials: structure, mechanical properties and applications of elastin and collagen proteins, Handb. Nanomater. Prop. (2014), doi:10.1007/978-3-642-31107-9.
[30] B. Aghaei-Ghareh-Bolagh, S.M. Mithieux, M.A. Hiob, Y. Wang, A. Chong, A.S. Weiss, Fabricated tropoelastin-silk yarns and woven textiles for diverse tissue engineering applications, Acta Biomater. 91 (2019) 112–122, doi:10.1016/j.actbio.2019.04.029.
[31] N. Annabi, S.M. Mithieux, A.S. Weiss, F. Dehghani, Cross-linked open-pore elastic hydrogels based on tropoelastin, elastin and high pressure CO2, Biomaterials 31 (2010) 1655–1665, doi:10.1016/j.biomaterials.2009.11.051.

[32] D.W. Urry, T. Hugel, M. Seitz, H.E. Gaub, L. Sheiba, J. Dea, J. Xu, T. Parker, Elastin: a representative ideal protein elastomer, Philos. Trans. R. Soc. B Biol. Sci. 357 (2002) 169–184, doi:10.1098/rstb.2001.1023.
[33] B. Aghaei-Ghareh-Bolagh, S. Mukherjee, K.M. Lockley, S.M. Mithieux, Z. Wang, S. Emmerson, S. Darzi, C.E. Gargett, A.S. Weiss, A novel tropoelastin-based resorbable surgical mesh for pelvic organ prolapse repair, Mater. Today Bio. 8 (2020) 100081, doi:10.1016/j.mtbio.2020.100081.
[34] L.D. Muiznieks, M. Miao, E.E. Sitarz, F.W. Keeley, Contribution of domain 30 of tropoelastin to elastic fiber formation and material elasticity, Biopolymers 105 (2016) 267–275, doi:10.1002/bip.22804.
[35] H.A. Scheraga, A. Liwo, S. Oldziej, C. Czaplewski, J. Pillardy, J. Lee, D.R. Ripoll, J.A. Vila, R. Kazmierkiewicz, J.A. Saunders, Y.A. Arnautova, K.D. Gibson, A. Jagielska, M. Khalili, M. Chinchio, M. Nanias, Y.K. Kang, H. Schafroth, A. Ghosh, R. Elber, M. Makowski, The protein folding problem, Lect. Notes Comput. Sci. Eng. 49 (2006) 90–100. doi: 10.1007/3-540-31618-3_6.
[36] C.J. Tsai, J.V. Maizel, R. Nussinov, Anatomy of protein structures: Visualizing how a one-dimensional protein chain folds into a three-dimensional shape, Proc. Natl. Acad. Sci. USA 97 (2000) 12038–12043, doi:10.1073/pnas.97.22.12038.